Characterization of fatigue delamination growth under mode I and II: Effects of load ratio and load history

G. Androuin[a], L. Michel[a,*], I. Maillet[b], X. Gong[a]

[a] *Institut Clément Ader (ICA), Université de Toulouse, ISAE-SUPAERO, UT3, IMT MINES-ALBI, INSA, CNRS, 3 rue Caroline Aigle, 31400 Toulouse, France*
[b] *DGA – Techniques Aéronautiques, Direction Générale de l'Armement (DGA), 47 rue Saint Jean, 31130 BALMA, France*

Keywords:
Fatigue
Delamination
Composites
Load ratio effect
Variable amplitude loads

A B S T R A C T

The study of fatigue delamination growth in composite materials aims to develop a slow-growth approach for composite materials that would provide conservative and reliable results. The present work focuses on the study of the load ratio effect on fatigue crack growth at constant amplitude and on the effect of variable amplitude loading on crack propagation. With this in mind, a Crack Driving Force (CDF) is chosen to attempt to overlap delamination growth curves obtained from different load ratio values for mode I and mode II. It is shown that the CDF collects the effect of the load ratio on the crack growth curves and allows to build a crack growth master curve for mode I and II. Variable amplitude loads are then considered for delamination propagation in mode I. However, variable amplitude loads bring to light a load history effect during fatigue crack growth that the CDF does not take into account.

1. Introduction

Within the context of damage tolerance in aircraft structures, the aircraft certification published by the Federal Aviation Administration (FAA) specifies: " The evaluation should demonstrate that the residual strength of the structure will reliably be equal to or greater than the strength required for the specified design loads (considered as ultimate), including environmental effects "[1]. Consequently, first, the critical size for delamination must be determined and second, the time required for the damage to reach its critical size when subjected to aircraft load spectra must be predicted. This research focuses on the latter phase. Within the context of damage tolerance in metallic structures, crack growth under spectrum loading is relatively well understood. The latter can be pre dicted using the Rainflow counting method for example, and taking into account delays related to the development of overloads in the load history [2]. However, concerning fatigue driven crack growth in carbon/epoxy composite materials, further study is re quired to determine whether such approaches are applicable. In fact, it is not yet fully understood how the different spectrum loading levels interact during growth. Due to their laminated, fibrous structure, the damage created at the delamination front of composite materials appears to be more complex than for a metallic material given that phenomena are more varied. A damage zone develops around the main crack front; it includes plastic deformation or micro cracking of matrix which extents lead to side cracks and fibre bridgings [3]. Furthermore, the type of organic matrix at the inter ply and in the ply, play an important role in terms of the matrix toughness of the laminate. For example, the polymeric nature of the matrix, thermoset or thermoplastic, modifies this property [4], as does the presence of nodules in the matrix [5]. According to the FAA on composite materials, the evaluation of default growth should

* Corresponding author.
E-mail addresses: guillaume.androuin@isae-supaero.fr (G. Androuin), laurent.michel@isae-supaero.fr (L. Michel), irene.maillet@intradef.gouv.fr (I. Maillet), xiaojing.gong@iut-tarbes.fr (X. Gong).

https://doi.org/10.1016/j.engfracmech.2018.06.030

Nomenclature

a	crack length
b	width of the specimen
C_0	constant compliance parameter
d	displacement
da/dN	crack growth rate
DCB	Double Cantilever Beam
F	force
G	Strain Energy Release Rate (SERR)
G_{max}	maximal SERR during a fatigue cycle
G_{min}	minimal SERR during a fatigue cycle
G_{Ic}	critical SERR in mode I
ΔG	load amplitude ($= G_{max} - G_{min}$)
$(\Delta\sqrt{G})^2$	load amplitude with respect to the similitude with K, $(\Delta\sqrt{G})^2 = (\sqrt{G_{max}} - \sqrt{G_{min}})^2$
K	stress intensity factor
K_{max}	maximum stress intensity factor during a fatigue cycle
K_{min}	minimum stress intensity factor during a fatigue cycle
k	constant in the Paris crack growth equation
m	exponent compliance parameter
n	exponent in the Paris crack growth equation
R	load ratio ($= d_{min}/d_{max}$)

give conservative and reliable results.

To describe fatigue driven crack growth, the Paris relation often adopts a power law and is formulated for composites as follows (Eq. (1)):

$$\frac{da}{dN} = k.\ G_{max}^{n} \tag{1}$$

where da/dN is crack growth rate, G_{max} is maximal strain energy release rate during a fatigue cycle and k and n are empirically determined parameters of the Paris Relation. Note that the strain energy release rate G is proportional to the load squared, and that this relation does not take into account either the effect of the average load, or load frequency. The average load can also be represented by load ratio R, defined as the ratio of the minimum load divided by the maximum load of the cycle. In addition, for small displacement assumption ($d_{max}/a < 0.4$), displacements remain linear to forces, and the load ratio can be written as the displacement ratio $R = d_{min}/d_{max}$ [6].

An aeronautics load spectrum is the result of an overlapping of loads from different flight phases such as takeoff, ascent and landing. Moreover, flight conditions such as gusts, and aeroelastic loads such as flutter also come into play. The spectrum parameters may vary greatly over time and the crack propagation may experience interaction between different load levels. Consequently, it is essential to verify if there is a load history effect when studying crack growth. This paper focuses on the effect of the load ratio and the average load, and their variation histories, on crack growth rate.

In the literature, several authors have described the effect of load ratio on fatigue crack growth and it has been shown that for a given value of G_{max}, the load ratio R significantly influences crack growth rate da/dN [7 14]. More specifically, the fatigue crack growth curves plotted for different load ratio values are parallel but shifted, and the shift direction depends on the quantity used as the X axis parameter: G_{max} or ΔG for example. These quantities can be seen as active principles which control the crack growth and will be generically denominated as Crack Driving Force (CDF) for the rest of the article. In fact, the curves resulting from the different load ratios are not overlapped for the same CDF. Consequently, a recurring problem is how to define a driving force of crack growth which would allow to plot a fatigue crack growth curve that does not depend on R, in particular by adjusting the definition of the CDF. Theoretically, this would enable to predict crack growth for a load spectrum in which the value of R varies, if the different load levels do not interact during crack growth.

Unlike the definition $\Delta K_{eff} = K_{max} - K_{eff}$, used for metallic materials to describe the effect of load ratio [15 18], the definition $\Delta G = G_{max} - G_{min}$, created by analogy, does not correctly take into account the effect of the load ratio [19]. This is due to the fact that the principle of similitude is not respected and the load ratio is defined as the coefficient of restitution $R = G_{min}/G_{max}$ rather than a force ratio, as is true for ΔK_{eff}.

The definition of Rans[19], used by Maillet[20], (Eq. (2)) re establishes this by setting this expression for $R = \sqrt{G_{min}}/\sqrt{G_{max}}$.

$$\begin{aligned}(\Delta\sqrt{G})^2 &= (\sqrt{G_{max}} - \sqrt{G_{min}})^2 \\ &= G_{max}(1-R)^2\end{aligned} \tag{2}$$

A load ratio effect R on da/dN cited in the literature can be related to the phenomenon of increased delamination resistance as a function of crack growth, called R curve. For growth under mode I, in a unidirectional carbon/epoxy composite, Yao and his co authors [13] observed that fracture surfaces formed during growth show more pronounced relief at high load ratio R. This increases resistance to growth and hence decreases growth rate. According to the authors, this could favor the development of fibre bridging and consequently help slow growth.

If a crack growth rate curve variation is plotted as a function of $(\Delta\sqrt{G})^2$ in the following manner: $Log(da/dN) = Log((\Delta\sqrt{G})^2)$, the crack growth curve is a straight line, which means that the Paris relation (Eq. (1)) applies. However, straight lines resulting from the different values of R are significantly shifted, while being nearly parallel. This means that the parameter n in the Paris relation (Eq. (1)) should be identical. Hence, it is possible to produce a master propagation curve, independent from the load ratio, by introducing a shift parameter, γ, according to the Eq. (3) [20].

$$
\begin{aligned}
\Delta G_{eq} &= (\sqrt{G_{max}} - \sqrt{G_{min}})^{2(1-\gamma)} G_{max}^{\gamma} \\
&= G_{max}(1-R)^{2(1-\gamma)}
\end{aligned} \tag{3}
$$

Unlike load ratio effect, there is relatively little in the literature on fatigue crack growth under variable amplitude loading on epoxy/carbon composite. Yao [21] performed fatigue testing under variable amplitude loading. The load profile is composed of two fatigue tests: the first one is carried out at $R = 0$ or $R = 0.5$ and the second at $R = 0.5$. Plotting the Fatigue Crack Growth Rate (FCGR) as a function of the maximum strain energy release rate (SERR) for the second block shows in both cases a propagation curve parallel to the first block. However, the growth rates of the second block of the load profile $R = 0.5/R = 0.5$ are significantly lower than those with the profile $R = 0/R = 0.5$. This could be explained by the development of more fibre bridging during the first block at $R = 0.5$, which would decrease the growth rates of the second block.

To assess the effect of load ratio on crack growth, the first section of this study focuses on constructing a master propagation curve for fatigue crack growth in mode I and in mode II for the material under consideration. To this end, four load ratios are considered in mode I, and respectively three load ratios in mode II, making it possible to identify the shift parameter γ. The second section of this paper deals with fatigue crack growth under variable amplitude loads in mode I. The experimental results show the importance of the load history effect. Using the linear Paris relation obtained in the first section of this study, an estimation of crack growth is obtained. The purpose is to determine whether the definition ΔG_{eq} is accurate enough to predict crack growth taking into account the potential load history effect.

2. Experimental conditions

2.1. Materials and specimens

Tests are carried out on the T700/M21 epoxy/carbon composite, provided by HEXCEL. Specimens are cut from plates measuring 400 $\times$300 mm^2, made from unidirectional stacking of 20 plies of T700/M21 pre pregs. The plates have then been autoclave poly merized respecting the manufacturer recommended curing cycle. Specimens dimensions are 180 ($\times$) 25 ($\times$) 5 mm^3 (length, width, thickness). A Teflon insert with a thickness of 25 µm is placed in the median plane to create an initial size default equal to 40 mm.

In mode I, tests are performed using a DCB test device. The loading tabs, the dimensions of which comply with the standard ASTM D5528 [22], are placed on the two edges of the crack to load the specimen in opening mode. An S100 crack gauge provided by RUMUL is then fixed on the edge of the specimen and connected to a Fractomat which provides a measurement of the crack length in real time. The fractomat resolution for a 100 mm gauge is given as ± 10µm.

In mode II, tests are performed using an ELS test device. Clamping of the specimen is insured by 2 screws tightened with a calibrated lever arm as specified in the Standard ISO 15114:2014 [23]. The load head is specifically designed to enable fatigue tests at negative load ratios. Specimens are graduated every millimeter on the edge to monitor the growth by observation during tests. The measurement incertainty is evaluated to 0.5 mm.

All specimens are pre cracked in mode I under static loading at a displacement rate of 0.1 mm/min to initiate the crack over a minimum of 2 mm. No specific conditioning was performed on specimens before tests. Tests were performed at Room temperature and Room humidity ratio.

2.2. Test devices

In mode I, fatigue tests are performed on a hydraulic machine at a frequency of 10 Hz, equipped with a load cell with a capacity of 200 N (Fig. 1). Required displacement Tests are performed. For these tests, force, displacement and length of the crack are constantly recorded.

In mode II, fatigue tests are performed on a hydraulic machine at frequency 1.5 Hz, equipped with a load cell with a capacity of 500 N (Fig. 2(a)). Imposed displacement tests are performed. For these tests, force and displacement are recorded. The size of the crack is monitored by dye penetrant: an ultraviolet reagent solution is introduced in the crack and spreads by capillary action along the crack. The test is interrupted every 200 cycles in maximum displacement position and a picture of the specimen section is taken.

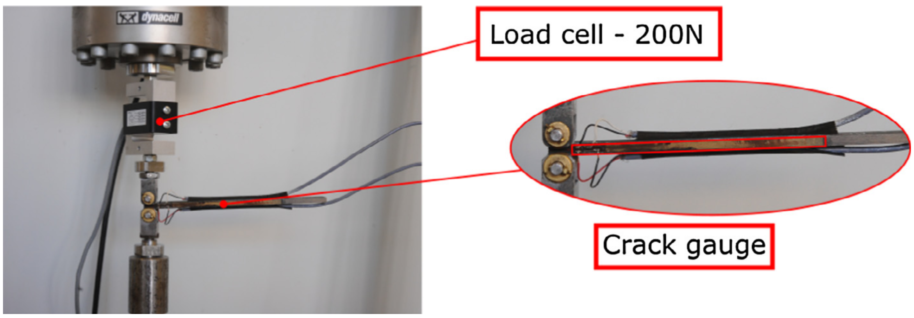

Fig. 1. DCB test device for fatigue in mode I.

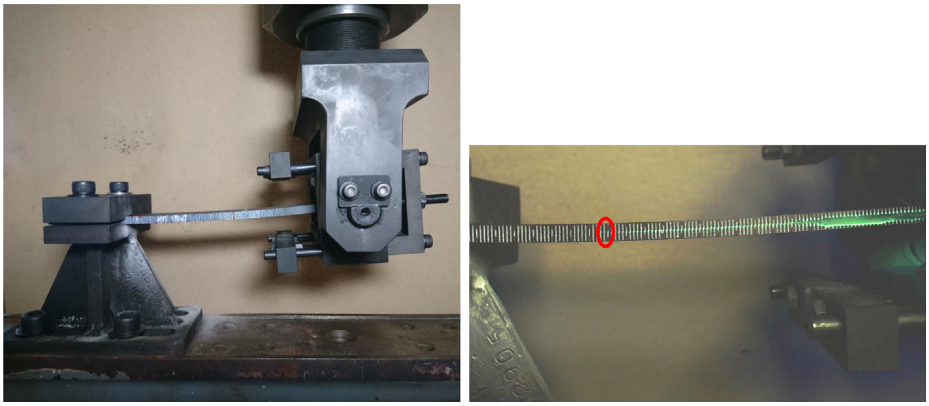

(a) ELT test device (b) $N = 25000$ cycles

Fig. 2. (a) ELS test device (b) example of picture taken during fatigue test and used to measure the crack extension.

This enables to determine the development of the crack length during the test. The crack front is identified on each picture (Fig. 2(b)). Initial and final crack length are always checked directly on the specimen before and after tests.

2.3. Data processing

2.3.1. Mode I

The maximum SERR is calculated using the compliance law. It is expressed by the Berry law $C = C_0 * a^m$ for each specimen. G_{max} is then calculated using the Irwin Kies formula (Eq. (4)):

$$G_{max} = \frac{P_{max}^2}{2b} \cdot \frac{\partial C}{\partial a} = \frac{m d_{max}^2}{2bC_0 a^{m+1}} \tag{4}$$

where d_{max} is the maximum displacement reached during the cycle, b is the specimen width, a the crack length and m and C_0 the formerly defined compliance parameters. Crack growth rate da/dN is calculated using the 7 points polynomial method in the Standard ASTM E647 05 [24]. When the crack growth rate is low (<10^{-6} mm/cycles), a smoothing is performed by averaging the crack length within a sliding window of 200 cycles. The acquisition frequency is defined at 300 Hz to have 30 measurement points per cycle which allows to measure the different required quantities: a, P_{max}, d_{max}.

2.3.2. Mode II

Experimental Compliance Method as presented in the Standard ISO 15114:2014 [23] has been used to calculate the value of the SERR. The crack length must be known at each cycle, while acquisition occurs every 200 cycles. Using the compliance expression in mode II $C = ma^3 + C_0$, it is possible to determine the crack length. To do so, specimen compliance at cycle N,

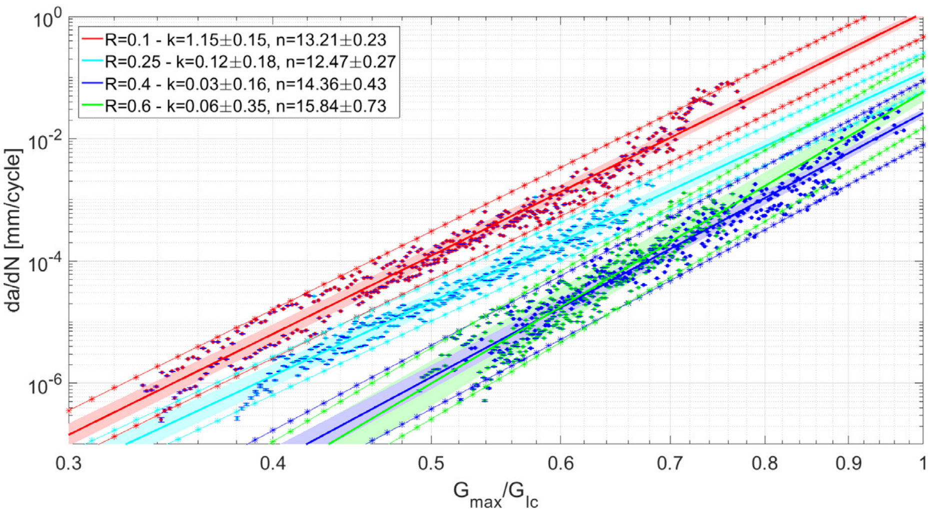

Fig. 3. Fatigue crack growth reference curves in mode I for $R = \{0.1;0.25;0.4;0.6\}$.

$C(N) = d_{max}(N)/F_{max}(N)$, allows to plot the development of C as a function of a^3. Compliance parameters m and C_0 are identified by linear fitting of this curve. For each cycle, crack length is interpolated by Eq. (5).

$$a(N) = \left[\left(\frac{d_{max}(N)}{F_{max}(N)} - C_0\right)\frac{1}{m}\right]^{\frac{1}{3}} \tag{5}$$

Smoothing of the crack length is performed by sliding window average over 1000 points (acquisition frequency is 300 Hz). Since the test crack growth rates are sufficiently low, this method may be used. This allows to calculate the SERR using the compliance law (Eq. (6)).

$$G_{max} = \frac{P_{max}^2}{2b}.\frac{\partial C}{\partial a} = \frac{3ma^2}{2b}.\frac{d_{max}^2}{(ma^3 + C_0)^2} \tag{6}$$

3. Results and discussion

Fatigue tests at constant load ratio were performed, using three specimens per load ratio. By defining maximum displacement as a test condition, the levels of the maximum SERR and crack growth rate decrease as the crack develops during the test.

3.1. *R effect on crack growth curves in mode I*

Crack growth curves obtained for the four load ratios $R = \{0.1;0.25;0.4;0.6\}$ are represented as follows (Fig. 3), where crack growth rate da/dN is plotted as a function of the maximum SERR G_{max} for a given value of R. For each load ratio, a power law is used to identify coefficients k and n, the values of which are specified in the legend. Whatever the curve considered, $Log(da/dN)$ varies linearly with $Log(G_{max})$. For each curve identified, it was decided to determine the influence of the measurements uncertainties on the calculation of G_{max} and da/dN, represented by horizontal and vertical error bars on each point.

A type B evaluation method was chosen to determine these measurement uncertainties. Characteristics of the different sensors or methods were used to estimate the measurement uncertainty of each initial quantity: load, crack length, specimen dimensions. An equally probable density was assumed to calculate standard uncertainties, and combined standard uncertainties were calculate for intermediate quantities such as the compliance C. Experimental compliance law was estimated with uncertainties and SERR un certainty calculated. Results show that these uncertainties are very small: roughly 3 N/m for calculation of G_{max} and roughly

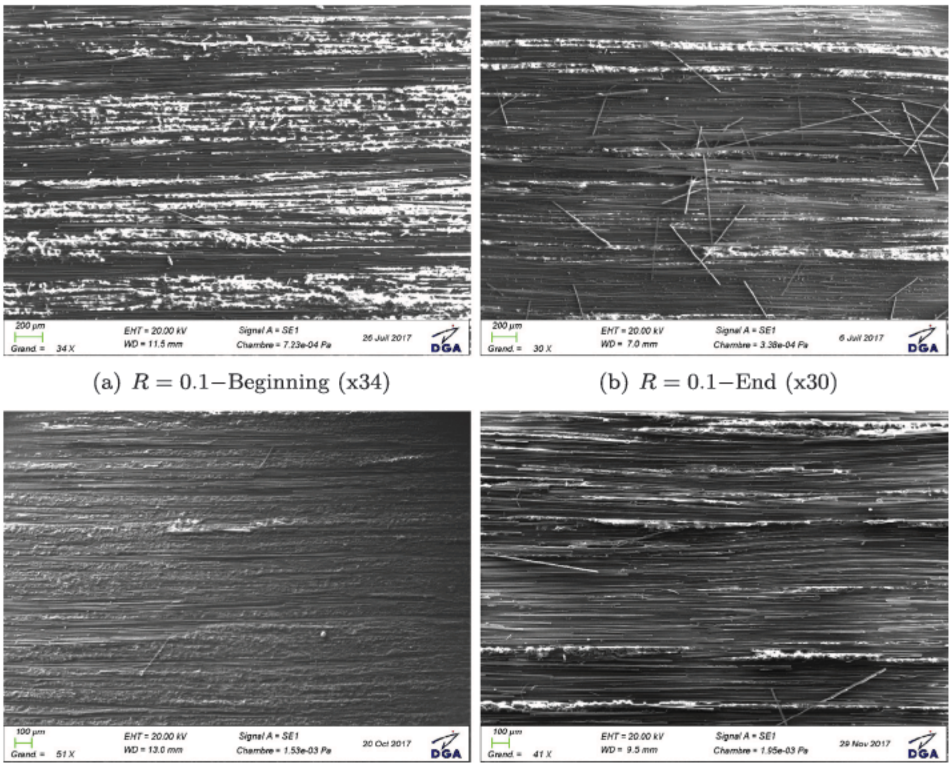

(a) $R = 0.1$–Beginning (x34)
(b) $R = 0.1$–End (x30)
(c) $R = 0.25$–Beginning (x51)
(d) $R = 0.25$–End (x41)

Fig. 4. SEM observations of fracture surfaces for $R = 0.1$ and $R = 0.25$ at the beginning and the end of the fatigue crack propagation.

10^{-8} mm/cycle for calculation of da/dN. Calculation uncertainties of da/dN is so low because the fractomat crack gauge presents a very low resolution.

In addition, calculation uncertainties of k and n are also determined. To do so, a statistical model is combined with the linear regression, allowing to determine calculation uncertainties over k and n by applying the central limit theorem via the law t of Student. These uncertainties are represented by colored zones in Fig. 3 for each curve identified. The exact crack growth curve is located in this zone with a 95% probability. Plus, a prediction interval is plotted (starred lines). A new experimental point has a 95% probability of being inside this interval.

It appears that the curves shift to lower crack growth rates when the load ratio R increases. Yao et al. [21] have reported an effect of the load ratio on the propensity for fiber bridgings. To investigate correlated phenomena on fracture surfaces, Scanning Electron Microscope (SEM) observations are carried out (Figs. 4 and 5). Specimens were machined 1 mm after the final crack front, then carefully opened to separate the two arms in order to preserve fracture surfaces. The crack propagation direction is along the horizontal of the micrographs and from the right to the left. SEM observations show the beginning and the end of the fatigue crack propagation zone. The beginning micrographs correspond to a zone located at about 1 mm from the precrack front. Observations made at the start of the fatigue crack zone correspond to a maximum SERR such as $G_{max} \approx 60\% Gc$ for all load ratios.

At the beginning of the crack growth (Figs. 4(a), (c), 5(a), (c)), fractography differs from the ones at end of the crack growth (Figs. 4(b), (d), 5(b), (d)) in the quantity of fibre debris. Fiber debris are spread over the surface for $R = 0.1$, whereas fewer and fewer debris are present with the increase of R at the end of the propagation. However, fibre failures appears on all fracture surfaces which mean that fiber bridging occurs at all load ratios. As identified in the literature, crack closure phenomenon occurs only for low load ratio values: Gustafson [25] observed it for $R = 0.1$ and Khan [9] did not observed it for R values such as $R > 0.3$. The crack closure phenomenon could thus explain the fibre debris observed for $R = 0.1$ since it may break fibre bridging in severals pieces. However, this quantity of fibre debris is not observed for $R = 0.25$, meaning that the crack closure phenomenon does not occur for and above that load ratio. These SEM observations make it possible to say that fibre bridging could develop with the crack propagation. This progress of the damage zone certainly plays a role in the crack growth rates and might lead to specific effects for delamination growth under variable amplitude loading.

In addition, Yao et al. [13] have concluded that there is a steady damage state for consecutive fatigue tests. Once it is reached, the damage state is saturated and can no longer exhibit further slow growth. It is possible that a similar phenomenon is involved for tests presented here: beyond $R = 0.4$, the crack growth curve shift is the same. This assumption is supported by SEM observations which show similar fracture surfaces for $R = 0.4$ and $R = 0.6$. There is a saturation position of the da/dN vs. G_{max} identified curves, beyond which the increase in load ratio does not result in additional shift.

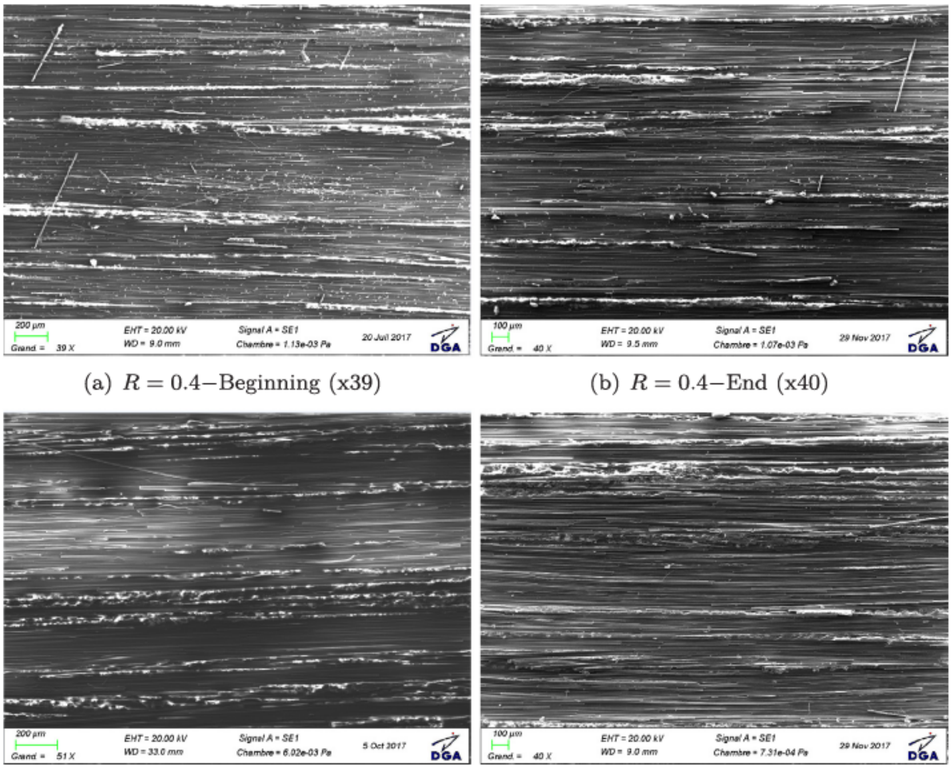

(a) $R = 0.4$–Beginning (x39) (b) $R = 0.4$–End (x40)

(c) $R = 0.6$–Beginning (x51) (d) $R = 0.6$–End (x40)

Fig. 5. SEM observations of fracture surfaces for $R = 0.4$ and $R = 0.6$ at the beginning and the end of the fatigue crack propagation.

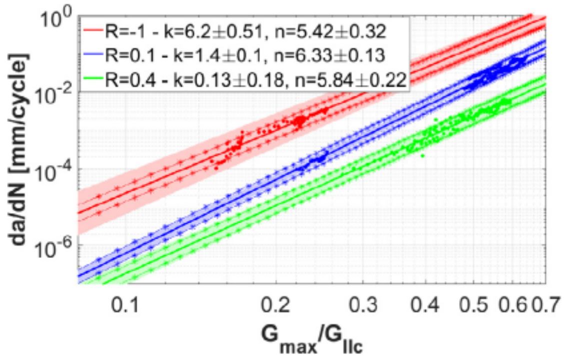

Fig. 6. Fatigue crack growth reference curves in mode II for $R = \{-1;0.1;0.4\}$.

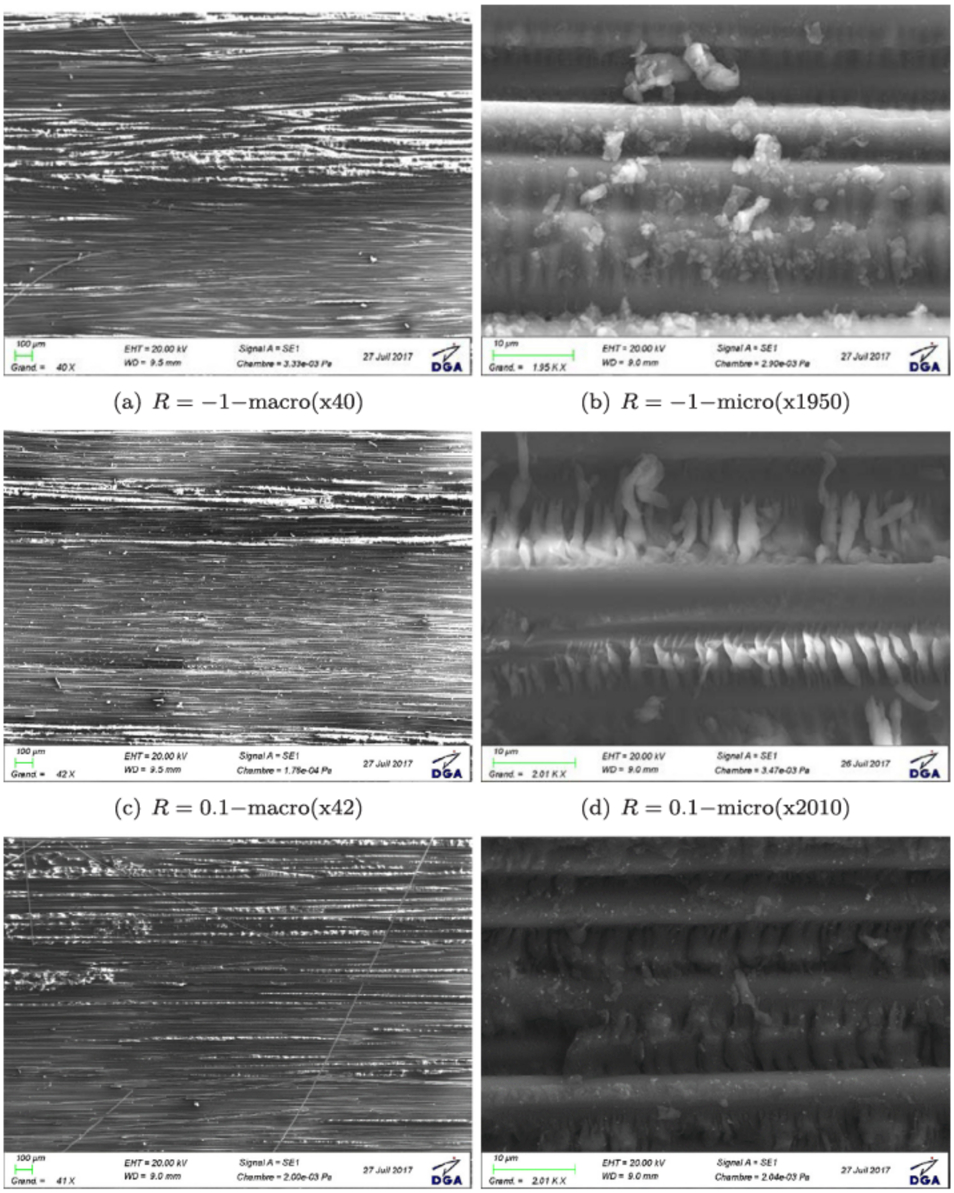

(a) $R = -1$–macro(x40)

(b) $R = -1$–micro(x1950)

(c) $R = 0.1$–macro(x42)

(d) $R = 0.1$–micro(x2010)

(e) $R = 0.4$–macro(x41)

(f) $R = 0.4$–micro(x2010)

Fig. 7. SEM observations of crack growth fracture surfaces in mode II for three load ratios, at high and low magnification.

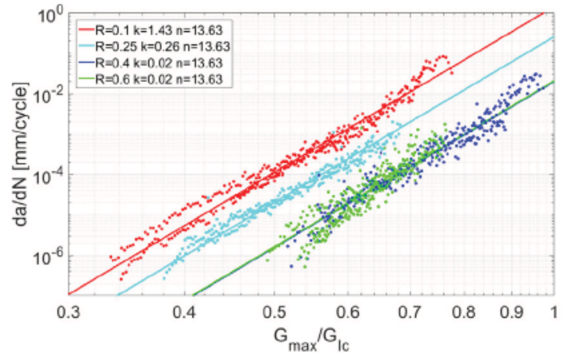

(a) Mode I

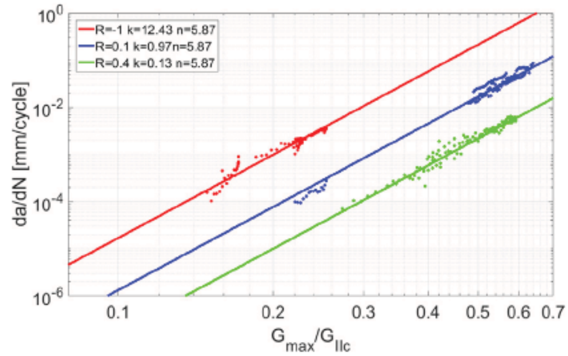

(b) Mode II

Fig. 8. Equalization of slopes by the least squared method for growth curves from different load ratios, for mode I and mode II.

3.2. *R effect on crack growth curves in mode II*

In mode II, three load ratios were tested $R = \{-1;0.1;0.4\}$. As in mode I, da/dN is plotted as a function of G_{max} (Fig. 6). Un certainties are plotted as in mode I.

The load ratio has the same effect on the crack growth curves as in mode I: a shift to lower crack growth rates is observed when the value of R increases. Fractography images are also taken for each load ratio at two different magnifications (Fig. 7).

Low magnification fractography pictures ($\sim\times 40$) show similar fracture surfaces for the three load ratios. At high magnification ($\sim\times 2000$), damage mechanisms are visible. However, given the frictions of the two arms of the cracked specimen in mode II, they are damaged and the fracture surface patterns are barely legible. The lower the value of R, the bigger the amplitude and the more the surface pattern looks damaged. However, it can be seen that the strips are rolled on themselves, which is due to the typical sliding load of mode II.

3.3. *Construction of a master curve independent from the load ratio*

For both modes, crack growth curves form nearly parallel lines which suggests that the results can be interpolated with a unique constant n of the linear Paris relation for all load ratios. However, the constant parameter k of the linear Paris relation seems to depend on load ratio R. As the slopes are close, the least squared method is used to equalize the slopes and obtain k and n for each load ratio. This serves as a basis for constructing a crack growth master curve (Fig. 8).

As seen above, the definition of ΔG_{eq} (Eq. (3)) is used as the crack driving force to construct the crack growth master curves in mode I and II. For each mode, the value of γ is determined by the least squared method applied to coefficients k of reference crack growth curves. The coefficients obtained for crack growth master curves (Fig. 9) are shown in the Table 1.

The effect of R is correctly integrated by the definition of the crack driving force ΔG_{eq} since for the two propagation modes, curves from the different load ratios are overlapping.

However it should be noted that the definition of ΔG_{eq} imposes a shift in the crack growth curves proportional to the load ratio value. In mode I, the position of reference curve $R = 0.4$ is considered to be a saturation position and the shift induced for the reference curve $R = 0.6$ is established equal to that of $R = 0.4$. In mode II, this phenomenon does not occur for the load ratio values explored.

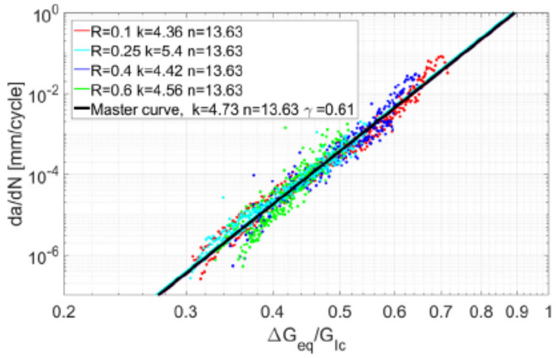

(a) Mode I

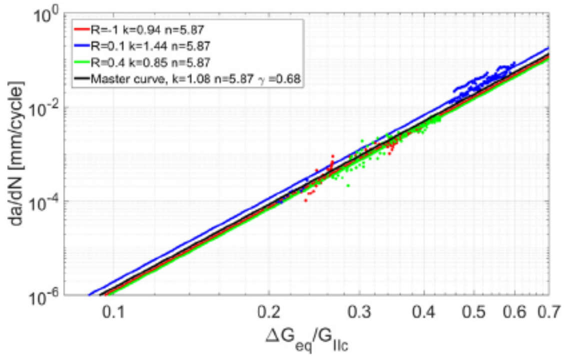

(b) Mode II

Fig. 9. Crack growth master curves independent from load ratio for modes I and II.

Table 1
Coefficients identified for the crack growth master curves in mode I and II.

Mode	k	n	γ
Mode I	4.73	13.63	0.61
Mode II	1.08	5.87	0.68

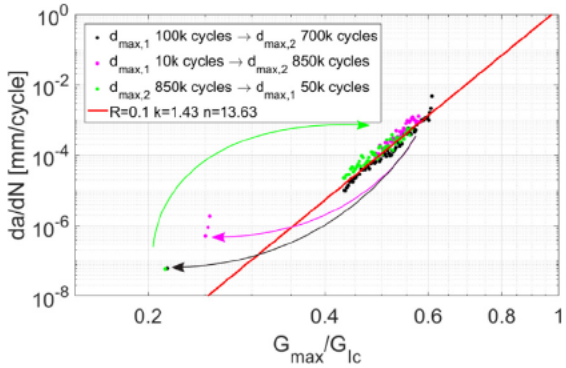

Fig. 10. Crack growth curves for loading composed of two blocks at different d_{max}.

3.4. Fatigue crack growth in mode I under variable amplitude loading

In this section, variable amplitude loading is considered. The purpose is to study the effect of the variation in load ratio and maximum displacement during a fatigue crack growth test in mode I. Two load programs are used: in the first one, the load ratio is constant while maximum displacement varies; in the second, the load ratio varies for a constant maximum displacement. The effects of these variations are observed in the crack growth curves, in comparison with those of the reference curves and the master curve

Table 2
Overview of variable amplitude loads for n blocks, at R constant and d_{max} variable.

Test	Block 1	Block 2	Repetitions
Test 1	10k cycles at $d_{max,1}$	50k cycles at $d_{max,2}$	13
Test 2	10k cycles at $d_{max,2}$	5k cycles at $d_{max,1}$	120

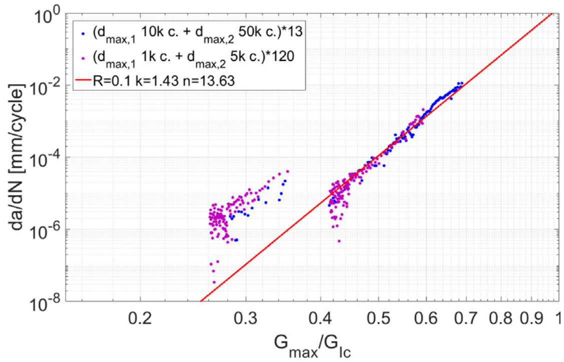

Fig. 11. Crack growth curves for an alternating load of blocks at $d_{max,1}$ and blocks at $d_{max,2}$ as a function of G_{max}/G_{Ic} with the reference curve $R = 0.1$.

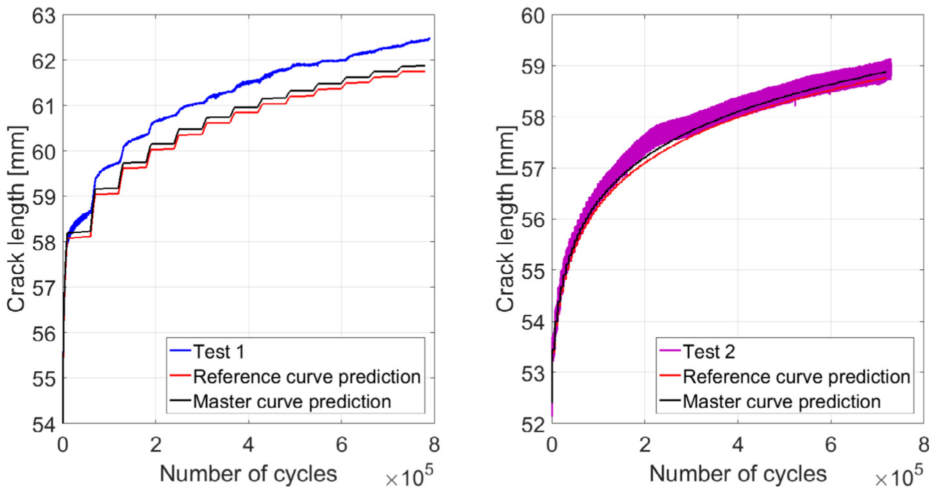

Fig. 12. Estimation of crack growth under load at constant load ratio and variable maximum displacement for the two cases considered: 2∗13 blocks (left) and 2∗120 blocks (right).

identified in the first section (Fig. 9(a)).

3.4.1. Loads at constant R and two levels of d_{max}

The load ratio is set at $R = 0.1$. Two levels of maximum displacement $d_{max,1}$ et $d_{max,2}$ are considered. They are determined such that $d_{max,1}$ and $d_{max,2}$ correspond to a given percentage of the critical energy restitution rate considering the size of the initial crack. Respectively here, at a maximum initial energy restitution rate $G_{1,initial} = 0, 6G_{Ic}$ and $G_{2,initial} = 0, 4G_{Ic}$, where G_{Ic} is the static SERR of the material in mode I. Then $d_{max,1} > d_{max,2}$.

Two blocks tests First, tests at two blocks were performed: the totality of cycles is divided into two blocks, one at $d_{max,1}$, the other at $d_{max,2}$. Two specimens are tested so as to obtain a block at maximum displacement $d_{max,1}$ first and another one so as to obtain a block at maximum displacement $d_{max,2}$ first (see legend). The results of these tests are shown in Fig. 10.

The red line copied from Fig. 8 represents the tests performed under constant loading at $R = 0.1$. It serves as a reference to situate the crack growth curves per block relative to tests under constant amplitude loading.

Whether the first block is at high $d_{max,1}$ or low $d_{max,2}$, the crack growth rates observed for the block at low level are much higher than the crack growth rates which would have been expected by using the constant amplitude linear Paris relation obtained before for $R = 0.1$ (red line). This difference might be due to a difference in the damage state extent at the delamination tip resulting from the progression of the delamination crack under either constant amplitude loading or variable amplitude loading.

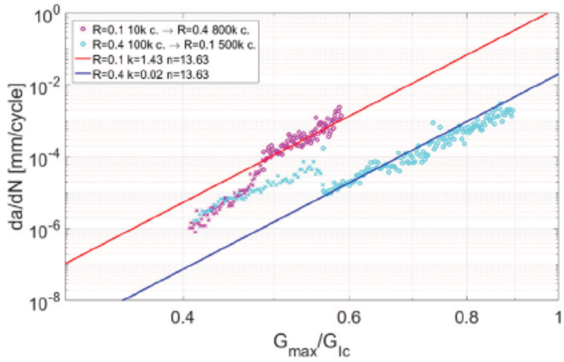

(a) da/dN vs. G_{max}/G_{Ic}

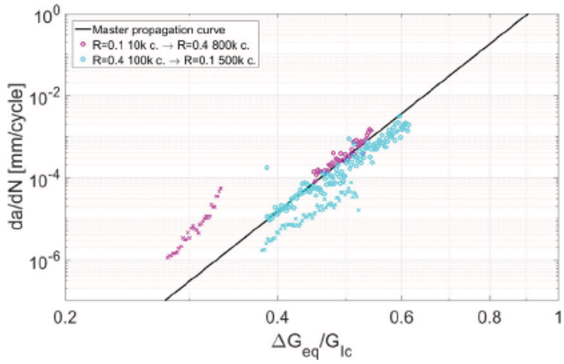

(b) da/dN vs. $\Delta G_{eq}/G_{Ic}$

Fig. 13. Crack growth curves for variable amplitude loads alternating one block at $R = 0.1$ and one block at $R = 0.4$. The marker change indicates the load ratio change.

Table 3
Overview of variable amplitude loads for n blocks, at R variable and d_{max} constant.

Test	Bloc 1	Bloc 2	Repetitions
Test 1	5k cycles $R = 0, 1$	15k cycles à $R = 0, 4$	42
Test 2	20k cycles à $R = 0, 4$	20k cycles à $R = 0, 1$	22

Sequence of two blocks repeated To complete this study, variable amplitude loads including several blocks at each level were used. The interest is to determine the evolution of the effect of the load history on crack curves when a sequence of two blocks is repeated several times. The load blocks are described in the following Table 2 and the crack growth curves obtained are presented in the Fig. 11).

Like for testing at two blocks, the phases corresponding to low levels of G_{max} show higher rates than that of the reference curve $R = 0.1$ which was obtained under constant amplitude. And, like for tests at two blocks, we think that this observation can be related to the extension of the damage zone at the delamination tip during fatigue loading. It has indeed been reported that the fiber bridging, or damage zone, develops with the crack propagation.

Because of the level jump to a lower energy G_{max} the crack propagates with a damage zone different from the one seen during the constant amplitude loading at the same energy. The damage at crack tip, which should have occurred if this low level of G_{max} had been reached through a crack propagation under constant amplitude, is not present. Yet it has been shown that fiber bridging is a shielding mechanism that slows crack growth. When the second block is at $d_{max,2}$, the crack growth rate is thus higher. When the first block is at $d_{max,2}$, the fiber bridging is not developed and the crack growth is hence not slowed.

At the end of the test, the blocks no longer contain enough cycles (from 1k to 50k) for the crack to grow enough to be correctly reported and an apparent saturation of the crack growth rate can be observed (Fig. 11).

This puts into question the way the Paris curve is obtained for low G_{max} levels, since the results might depend upon the loading history used to process the curve.

Crack growth reconstruction Based on the Paris coefficients of the reference curve at $R = 0.1$ and those of the master curve, the crack growth can be rebuilt and compared to that which was experimentally obtained (Fig. 12).

Both for tests 1 and 2, the crack growth estimations underestimate the real growth. As the crack growth master curve is close to the reference curve $R = 0.1$, the estimations realized are close. The difference between the experimental curve and the rebuilt curve is

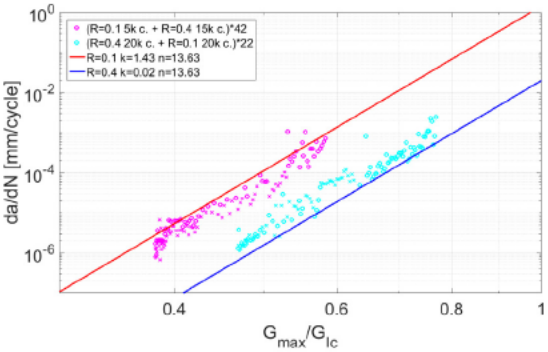

(a) da/dN vs. G_{max}/G_{Ic}

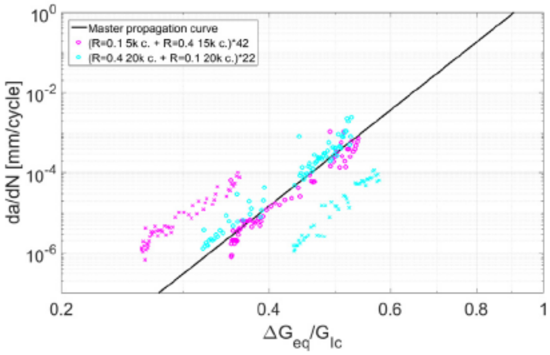

(b) da/dN vs. $\Delta G_{eq}/G_{Ic}$

Fig. 14. Crack growth curves for loading at two load ratios, $R = 0.1$ and $R = 0.4$, and several blocks at each load ratio.

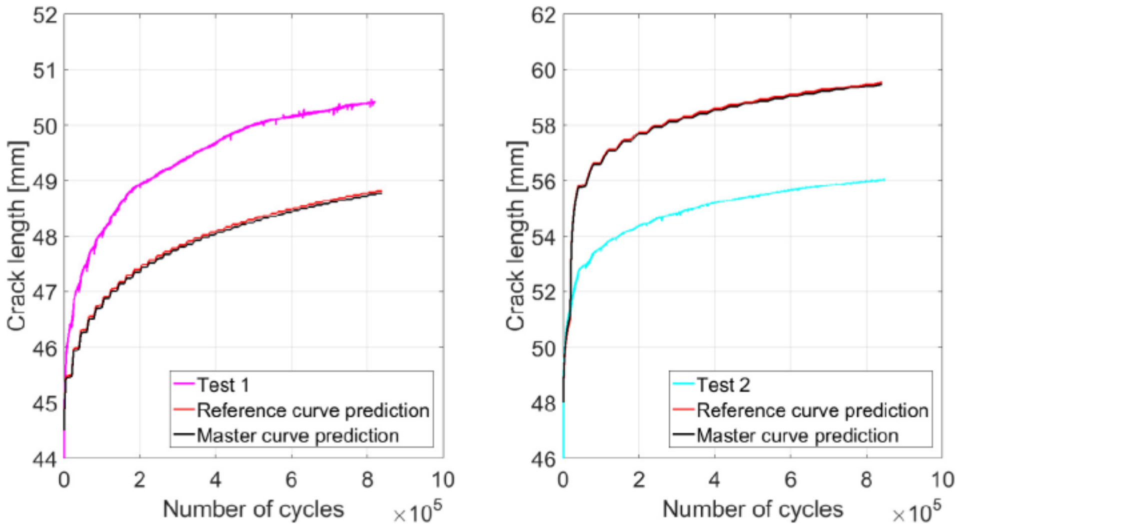

Fig. 15. Estimation of crack growth under variable load ratio and constant maximum displacement for the two cases considered: 2∗22 blocks (left) and 2∗42 blocks (right).

due to the estimation of the crack growth on low level blocks $d_{max,2}$. The growth estimation takes into account the crack growth rate of the reference curve, when the real crack growth rate is larger by at least one order of magnitude. This difference is very significant at the start of the growth, when the rates are high and it disappears with crack growth, since the rates are lower and lower. For test 2, the difference is less marked since the blocks are shorter, and hence the crack grows less during low level phases.

3.4.2. *Loads at d_{max} constant and two levels of R*

In this section, tests are performed at constant maximum displacement. The load ratio alternates between two values $R = 0.1$ and $R = 0.4$. In the same way as previously described, loads at two blocks are first used. The crack growth data are expressed with

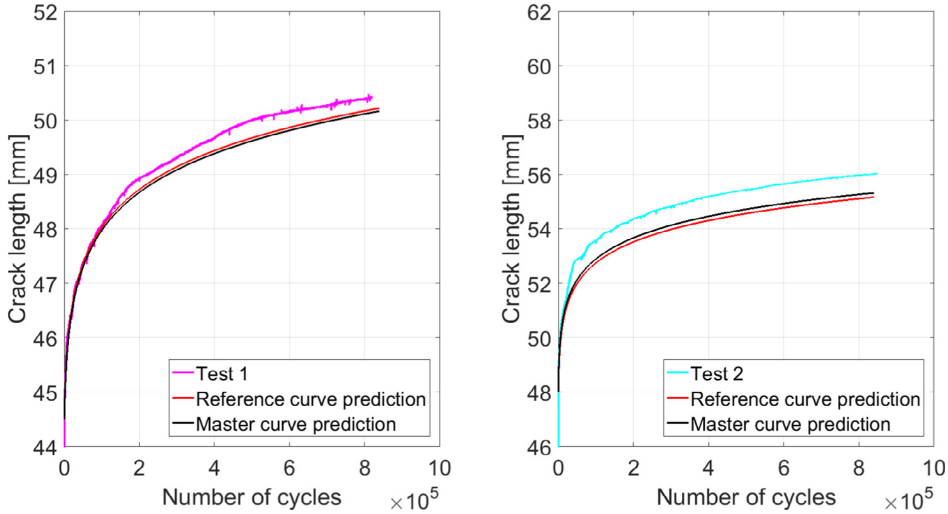

Fig. 16. Estimation of crack growth under variable load ratio and constant maximum displacement considering a single load ratio.

G_{max}/G_{Ic} but also as a function of $\Delta G_{eq}/G_{Ic}$ since the crack growth master curve is assumed to reflect the effect of the load ratio. The resulting growth curves are represented on the figure below (Fig. 13), where the marker change (crosses and circles) indicates the block change in the load. The red and blue lines are respectively the reference curves at $R = 0.1$ constant and $R = 0.4$ constant of the first part (Fig. 8).

The crack growth curves obtained for loading at two blocks show clearly a load history effect (Fig. 13(a)). When the first block is at $R = 0.1$, the second block at $R = 0.4$ shows much higher crack growth rates than the reference curve at $R = 0.4$. If there were no load history effects, the latter block should be on the reference curve at $R = 0.4$. An effect when the first block is at $R = 0.4$ can also be observed: the crack growth rates of the second block are lower than those of the reference curve at $R = 0.1$. This is more visible on the Fig. 13(b), where the growth data are plotted as a function of ΔG_{eq}. The first blocks are clearly situated on the crack growth master curve as they are not impacted by a load history. However, the second blocks are both shifted from this curve: towards higher rates for the block at $R = 0.4$ and towards lower rates for the block at $R = 0.1$.

It may be supposed that the block at load ratio $R = 0.4$ builds more resistance to crack propagation. This would explain the crack propagation rates decrease at the transition for a $R = 0.1$–$R = 0.4$ load program. Similarly, the crack growth rate is increased at the transition for a $R = 0.4$–$R = 0.1$ load program.

In the same way as previously described, fatigue tests at several blocks of each load ratio are performed (Table 3). The crack growth curves obtained are shown in Fig. 14.

For the two tests, the effect previously observed for two blocks can be seen again. The transition from one block $R = 0.1$ to a block $R = 0.4$ decreases the crack growth rate while the inverse transition increases it (Fig. 14). However, the interest of these two tests lies in the position of the crack growth curves obtained. If the load ratio of the first block is $R = 0.1$, then the crack growth curve "will follow" the reference curve of this load ratio. The same scenario occurs in the case when the first block is at $R = 0.4$.

It is possible to simulate the crack growth (Fig. 15). This uses again the crack growth rates of reference curves $R = 0.1$ and $R = 0.4$ for the associated blocks.

Both for the test starting with a block at $R = 0.1$ or the test starting by a block at $R = 0.4$, the estimations are skewed by the load history effect. In the first case, the growth is under estimated since the blocks at $R = 0.4$ present crack growth rates much higher than those of the reference curve at $R = 0.4$. In the second case, the growth is overestimated since this time, the blocks are at $R = 0.1$ which present lower crack growth rates than those of the reference curve at $R = 0.1$. In view of the crack growth curves, the crack growth estimation is potentially better if it is performed with the load ratio reference curves of the first block, in other words that it is considered that the blocks are all carried out at the load ratio of the first block. In this case, the crack growth estimations become those shown in Fig. 16.

The estimation of the crack growth is effectively better when a single load ratio is considered. However, the estimations are not conservative when the load ratio of the first block is the lowest.

4. Conclusions and perspectives

First, the effect of the load ratio has been demonstrated for the material used, and shows that at a given G_{max}, an increase in R results in a decrease in crack growth rate. The Paris slope identified is however similar from one load ratio to another. SEM ob servations show that the damage develops with the crack propagation and thus decreases the crack growth rate. Using the definition ΔG_{eq}, a crack growth master curve independent from the load ratio was plotted. In case of constant amplitude loading, this curve can be used to simulate the crack propagation. The question remains if it can be used in the case of variable amplitude loading.

To verify this assumption, tests were performed for loads alternating blocks either at variable d_{max} and constant R or at d_{max}

constant and R variable. The tests highlighted the effect of load history. In the first case, the load history effect is weak, where blocks made at the weaker d_{max} show faster rates than those of the reference curve. In the second case, it was shown that the crack growth curve followed the load ratio reference curve of the first block, which reflects the important effect of the load history. This shows that the obtained crack growth master curve cannot simulate the crack propagation for variable amplitude loading.

FAA requires conservative and reliable results for the slow growth characterization for composite structures. The question re mains to include correctly the effect of variable amplitude loading in the determination of a conservative and reliable crack growth curve for low crack growth rates.

Acknowledgments

This work is supported by the DGA (Délégation Générale de l'Armement, French ministry of Defence) and the Occitanie region.

References

[1] Federal Aviation Administration. Advisory Circular. Tech. Rep. 20-107B. U.S. Department of Transportation; 2009.
[2] Downing SD, Socie DF. Simple rainflow counting algorithms. Int J Fatigue 1982.
[3] Friedrich K, Walter R, Carlsson LA, Smiley AJ, Gillespie JW. Mechanisms for rate effects on interlaminar fracture toughness of carbon/epoxy and carbon/PEEK composites. J Mater Sci 1989;24(9):3387–98.
[4] Lachaud F, Lorrain B, Michel L, Barriol R. Experimental and numerical study of delamination caused by local buckling of thermoplastic and thermoset composites. Compos Sci Technol 1998(58):727–33.
[5] Kinloch AJ, Shaw SJ, Tod DA, Hunston DL. Deformation and fracture behaviour of a rubber-toughened epoxy: 1. Microstructure and fracture studies. Polymer 1983;24(10):1341–54.
[6] ASTM-D6115-97(2011). Standard test method for mode I fatigue delamination growth onset of unidirectional fiber-reinforced polymer matrix composites. ASTM International. West Conshohocken, PA; 2011.
[7] Hojo Masaki, Tanaka Keisuke, Gustafson Claes Göran, Hayashi Ryuichi. Effect of stress ratio on near-threshold propagation of delamination fatigue cracks in unidirectional CFRP. Compos Sci Technol 1987;29:273–92.
[8] Hojo M, Ando T, Tanaka M, Adachi T, Ochiai S, Endo Y. Modes I and II interlaminar fracture toughness and fatigue delamination of CF/epoxy laminates with self-same epoxy interleaf. Int J Fatigue 2006;28(10):1154–65. http://dx.doi.org/10.1016/j.ijfatigue.2006.02.004.
[9] Khan Rafiullah, Alderliesten René, Yao Liaojun, Benedictus Rinze. Crack closure and fibre bridging during delamination growth in carbon fibre/epoxy laminates under mode I fatigue loading. Compos A: Appl Sci Manuf 2014;67:201–11. http://dx.doi.org/10.1016/j.compositesa.2014.08.028.
[10] Mall S. Stress ratio effect on cyclic debonding in adhesively bonded composite joints. Compos Struct 1987(8):31–45.
[11] Donough MJ, Gunnion AJ, Orifici AC, Wang CH. Scaling parameter for fatigue delamination growth in composites under varying load ratios. Compos Sci Technol 2015;120:39–48. http://dx.doi.org/10.1016/j.compscitech.2015.10.011.
[12] Atodaria DR, Putatunda SK, Mallick PK. A fatigue crak growth model for random fiber composites. J Compos Mater 1997;31(18):1838–55.
[13] Yao Liaojun, Alderliesten RC, Benedictus R. Interpreting the stress ratio effect on delamination growth in composite laminates using the concept of fatigue fracture toughness. Compos A: Appl Sci Manuf 2015;78:135–42. http://dx.doi.org/10.1016/j.compositesa.2015.08.005.
[14] Hu W, Jones R, Kinloch AJ. Discussion of the stress ratio effect on the fatigue delamination growth characterization in frp composite structures. Vol. 2. Procedia Struct Integrity; 2016. p. 66–71.
[15] Dubey S, Soboyejo ABO, Soboyejo WO. An investigation of the effects of stress ratio and crack closure on the micromechanisms of fatigue crack growth in Ti-6Al-4V. Acta Materialia 1997;45(7):2777–87.
[16] Liaw Peter K, Leax TR, Swaminathan VP, Donald JK. Influence of load ratio on near-threshold fatigue crack propagation behavior. Scripta Metallurgica 1982;16(7):871–6.
[17] Minakawa K, Nakamura H, McEvily AJ. On the development of crack closure with crack advance in a ferritic steel. Scripta Metallurgica 1984;18(12):1371–4.
[18] Elber W. Fatigue crack closure under cyclic tension. Eng Fract Mech 1970;2(1):37–45.
[19] Rans Calvin, Alderliesten René, Benedictus Rinze. Misinterpreting the results: how similitude can improve our understanding of fatigue delamination growth. Compos Sci Technol 2011;71(2):230–8. http://dx.doi.org/10.1016/j.compscitech.2010.11.010.
[20] Maillet Iréne, Michel Laurent, Souric Frédéric, Gourinat Yves. Mode II fatigue delamination growth characterization of a carbon/epoxy laminate at high frequency under vibration loading. Eng Fract Mech 2015;149:298–312. http://dx.doi.org/10.1016/j.engfracmech.2015.08.030.
[21] Yao Liaojun, Sun Yi, Zhao Meiying, Alderliesten RC, Benedictus R. Stress ratio dependence of fibre bridging significance in mode I fatigue delamination growth of composite laminates. Compos A: Appl Sci Manuf 2017;95:65–74. http://dx.doi.org/10.1016/j.compositesa.2016.11.030.
[22] ASTM-D5528-13. Standard test method for mode I interlaminar fracture toughness of unidirectional fiber-reinforced polymer matrix composites. ASTM International. West Conshohocken, PA; 2013.
[23] ISO-15114:2014. Fibre-reinforced plastic composites – determination of the mode II fracture resistance to unidirectionnally reinforced materials using the calibrated end-loaded split (C-ELS) test and an effective crack length approach; 2014.
[24] ASTM-E647-05. Standard test method for measurement of fatigue crack growth rates. ASTM International. West Conshohocken, PA; 2014.
[25] Gustafson Claes-Göran, Hojo Masaki. Delamination fatigue crack growth in unidirectional graphite/epoxy laminates. J Reinforced Plast Compos 1987;6(1):36–52. http://dx.doi.org/10.1177/073168448700600104.